Detection of acoustic second harmonics in solids using a heterodyne laser interferometer

Moreau, A.

Publisher's version / Version de l'éditeur:
https://doi.org/10.1121/1.413240
Journal of the Acoustical Society of America, 98, 5, pp. 2745-2752, 1995

Detection of acoustic second harmonics in solids using a heterodyne laser interferometer

A. Moreau
Industrial Materials Institute, National Research Council of Canada, 75 boul. de Mortagne, Boucherville, Québec J4B 6Y4, Canada

(Received 6 October 1994; accepted for publication 6 June 1995)

Acoustic second harmonic generation in solids is difficult to measure and often requires careful sample preparation. In this paper, a heterodyne interferometer modified to measure acoustic fundamental and second harmonics is presented. It requires relatively little sample preparation and it provides noncontact, wideband, absolute, and pointlike measurements. It is shown that the output of an ideal heterodyne interferometer does not contain any even harmonics of a single-frequency acoustic signal. Odd harmonics, however, are produced in calculable amounts. A detailed model of the interferometer is introduced to account for various sources of spurious second harmonics and the model is experimentally verified. Three methods of calibration for the absolute measurement of surface displacement are presented. Measurements of the nonlinearity parameter, β, of a fused quartz sample are shown to agree with literature values.

PACS numbers: 43.25.Dc, 43.25.Zx, 43.58.Ry

INTRODUCTION

Nonlinear acoustic measurements can provide information on the microstructure or internal state of stress of materials, and may permit their nondestructive characterization.[1] But nonlinear effects are difficult to measure, especially in industrial environments. For example, changes in acoustic velocity with temperature or with applied stress are small and temperature and stress are often difficult to vary. Other techniques based on the detection of acoustic harmonics,[2] the interaction of multiple acoustic wavefronts,[3] and acoustic-radiation-induced static strain[4] require sensitive transducers calibrated for absolute amplitude measurements. The absolute calibration is necessary to determine the material's third-order elastic constants. Of these techniques, detecting second harmonics may be the most practical because no applied stress, no (slow) change in temperature, and only one acoustic source are used.

Acoustic second harmonic generation in solids is often studied using a capacitive transducer[5] as a detector because detectors able to measure absolute displacements with good sensitivity, wide dynamic range, and wide bandwidth are required. For example, a 10-MHz, 40-Å amplitude, 6000-m/s longitudinal acoustic wave propagating a distance of 1 cm in a material with a nonlinearity parameter, β, of 5, develops a 20-MHz second harmonic of 0.1-Å amplitude. Capacitive transducers, however, require time-consuming sample preparation and can only be implemented in the laboratory.

Light diffraction techniques have been widely used to study harmonic generation of surface acoustic waves. The surface waves create a diffraction grating upon which a light probe is reflected with several intensity peaks.[6] By measuring the amplitude of the various diffraction peaks, the second- and higher-order acoustic harmonic amplitudes can be obtained. Several other optical techniques specific to surface acoustic waves are described in the literature.[7] These techniques are effective in establishing the diffraction patterns of surface waves and for observing the growth of second- and higher-order harmonics. But they cannot be applied to bulk waves.

Optical detection of acoustic second harmonics using interferometric techniques[8–11] may be an interesting alternative. In addition to providing absolute values of the displacement, wide dynamic range, and wide bandwidth, they are noncontact methods, require little or no sample preparation, and provide quick measurements. Their main disadvantage is reduced but adequate sensitivity. In contrast to capacitive techniques, which average the acoustic field over a large area, optical interferometers can detect acoustic displacements at a single point.

In this paper, a heterodyne interferometer modified to measure acoustic second harmonics is presented. It is shown that the output of an ideal heterodyne interferometer does not contain any even harmonics of a single-frequency acoustic signal. Odd harmonics, however, are produced in calculable amounts. A detailed model of the interferometer is introduced to account for various sources of spurious second harmonics and the model is experimentally verified. Measurements of the nonlinearity parameter, β, of a fused quartz sample are shown to agree with literature values.

I. THE "IDEAL" HETERODYNE MICHELSON INTERFEROMETER

In a previous paper,[12] it is shown that both homodyne and heterodyne interferometers can be configured to yield an electrical output proportional to the sine of the optical phase shift induced by an acoustic displacement of the sample surface. Although the heterodyne interferometer is conceptually more complicated than the homodyne interferometer, it was chosen because it provides improved isolation against mechanical vibrations and variations in the reflected light intensity.

We utilize a commercial Michelson interferometer

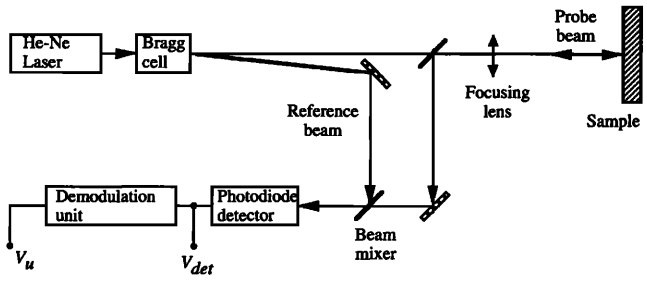

FIG. 1. Schematics of the Ultra-Optec OP35 heterodyne interferometer. The output signal V_u is proportional to the surface displacement.

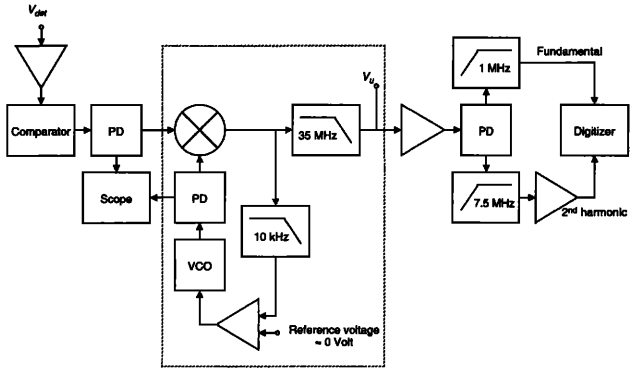

FIG. 2. Electronic demodulation and processing of the detected signal for a 5-MHz acoustic wave. Items identified as "PD" are power dividers and "VCO" is a voltage-controlled oscillator. The section within the dotted box performs the phase demodulation.

(Ultra-Optec OP35-O) described in the literature.[13,14] In the schematic diagram shown in Fig. 1, the reference beam is frequency-shifted using a 40-MHz acousto-optic modulator (Bragg cell). The interference of the reference beam and of the probe beam reflected from the sample surface causes a 40-MHz variation of the light intensity at the photodiode detector. Fluctuations in the path difference between the two beams, caused by ultrasonic displacements of the sample surface, phase-modulate the detected light intensity. The detected signal V_{det} is

$$V_{\text{det}}=A\cos(\omega_B t+4\pi U(t)/\lambda)=A\cos(\omega_B t+\varphi(t)), \quad (1)$$

where A is a proportionality constant, λ is the wavelength of light, and $U(t)$ and $\varphi(t)=4\pi U(t)/\lambda$ are the acoustic displacement and probe-beam phase shift as a function of time t, and ω_B is the frequency of the modulation (Bragg frequency).

To extract the acoustic information, V_{det} is mixed with another signal of frequency ω_B, but in quadrature:

$$V_{\text{det}}\sin\omega_B t=A\cos(\omega_B t+\varphi(t))\sin\omega_B t. \quad (2)$$

This equation is expanded and all terms with frequencies above ω_B are neglected (they are electronically filtered out). The output signal V_u is

$$V_u=-(A/2)\sin\varphi(t)\approx-(A/2)\varphi(t), \quad (3)$$

where the last approximation is valid for $\varphi\leqslant 1$, i.e., for acoustic displacements much smaller than the optical wavelength. The demodulated signal is linear in the surface displacement to first order. To higher orders, only odd powers of $\varphi(t)$ are present, and in amounts proportional to the Taylor expansion coefficients of the sine function.

The electronic implementation of this demodulation scheme is shown in Fig. 2. A mixer is used as the multiplicative element between V_{det} and a quadrature signal generated by a voltage controlled oscillator (VCO). The output 35-MHz low-pass filter eliminates all frequencies above ω_B. A 10-kHz feedback loop maintains the 90° phase relationship between V_{det} and the quadrature signal in the presence of ambient vibrations. This method of compensation is more effective than the actuated mirror of the homodyne interferometer because it does not involve an electromechanical feedback loop of limited bandwidth caused by mirror mass and piezoelectric resonances. A second advantage of this demodulation scheme is ease of calibration. The proportionality constant A of Eq. (3) can easily be determined by unlocking the phase-locked loop. The circuit's output V_u then settles to some frequency equal to $|\omega_B-\omega_{\text{VCO}}|$. As the relative phase of the two mixer inputs goes through 2π, the output of the interferometer is a sine wave of amplitude $A/2$.

For a sinusoidal acoustic signal of the form $U(t)=U_1\sin\omega_u t$ and writing $\varphi_1=4\pi U_1/\lambda$, V_{det} of Eq. (1) can be expanded into its frequency components as follows (the proportionality constant A is neglected for simplicity):

$$V_{\text{det}}=\cos\omega_B t\cos(\varphi_1\sin\omega_u t)-\sin\omega_B t\sin(\varphi_1\sin\omega_u t)$$

$$=\sum_{s=-\infty}^{\infty}J_s(\varphi_1)\cos(\omega_B+s\omega_u)t, \quad (4)$$

where the following identities are used:

$$\cos(x\sin\theta)=J_0(x)+2\sum_{i=1}^{\infty}J_{2i}(x)\cos(2i\theta),$$

$$\sin(x\sin\theta)=2\sum_{i=1}^{\infty}J_{2i-1}(x)\sin((2i-1)\theta), \quad (5)$$

$$J_{-i}(x)=(-1)^i J_i(x).$$

Equation (4) shows that the phase-modulated light signal contains a carrier frequency and an infinite number of lateral sidebands, the sth sideband having a relative amplitude $J_s(\varphi_1)$. These relative sideband amplitudes of the detected signal are easily measured on a spectrum analyzer. The demodulated and low-pass filtered output of this signal becomes

$$V_{\text{det}}\sin\omega_B t=\sin\omega_B t\sum_{s=-\infty}^{\infty}J_s(\varphi_1)\cos(\omega_B+s\omega_u)t,$$

$$V_u=-\sum_{s=1,s\ \text{odd}}^{\omega_B/\omega_u}J_s(\varphi_1)\sin s\omega_u t. \quad (6)$$

Equation (6) shows that the electronics do not generate any even harmonics of the acoustic signal. Only odd harmonics are produced in amounts proportional to $J_s(\varphi_1)$, where s is the order of the harmonic. Unlike Eq. (3), this result is not restricted to small acoustic displacements.

II. THE NONIDEAL INTERFEROMETER

Unfortunately, many experimental factors complicate this simple analysis. There are many potential sources of spurious second harmonics and each one must be given careful consideration. This section presents these sources in the order they appear during signal processing.

A. Amplitude modulation of the photodetector's output

Sample surfaces are generally rough and the amount of light collected may vary from point to point on the surface. Alternatively, a mirrorlike surface may not be flat and the optics may become misaligned as the sample is translated in front of the probe. Consequently, the calibration of the interferometer may apply only to a specific location. Moreover, an ultrasonic wave arriving at the sample surface with an oblique incidence angle may cause the probe beam to be reflected with a time varying angle so that the interferometer's optics may move in and out of alignment.

In fact, it is observed that the output of the photodiode, V_{det}, is both phase and amplitude modulated by the acoustic signal. It is difficult to understand the source of this phenomenon. Electromagnetic feedthrough is rejected because the amplitude modulation is approximately correlated in time with the arrival of the acoustic wave, and not with the electrical excitation of the generation transducer. By blocking the reference beam and positioning the photodiode so that only half the reflected beam falls onto the detector's active area (such as in a knife edge technique[15]), a signal varying at the excitation frequency is observed which indicates that the probe beam is reflected at a time varying angle. Note that even if the beams are well centered on a sufficiently large detector (and on every optical component), an amplitude modulation of the carrier can be observed because the varying reflection angle of the returning beam may cause the two beams to be relatively misaligned and to interfere with a varying amplitude. The reference beam acts as an aperture of finite dimensions.

Although these explanations appear reasonable, it is not known how the acoustic wave could cause a time-varying reflection angle of the light probe. A lithium niobate transducer is bonded to a suprasil W1 sample with a thin layer of oil and generates a longitudinal wave which travels to the opposite surface. This surface is coated with a thin layer of Al (≈ 1 μm) to improve its reflectivity and with a thin SiO_2 protective overcoat. The light probe is in the axis of the transducer. In this geometry, the longitudinal acoustic wave should make the surface vibrate as a whole, in the normal direction and without any angular variations. Surface defects or dust particles should not move in and out of the probed region as they might for a shear wave. Oblique incidence waves and non-normal displacements, however, may occur due to transducer edge waves or reflections from the sides of the sample. This could cause a tilt of the surface and the observed time-varying reflection angle. Further work will be required to explain quantitatively the origin of this amplitude modulation. We have not investigated this effect further because the amplitude modulation can be removed by electronic processing, as will be seen below.

Some consequences of this amplitude modulation can be derived. For amplitude modulation and acoustic displacements of the form

$$A(t)=A_0+A_1\cos(\omega_u t+\phi),$$
$$U(t)=U_1\sin\omega_u t, \tag{7}$$

Eq. (4) becomes

$$V_{\text{det}}=(A_0+A_1\cos(\omega_u t+\phi))\sum_{s=-\infty}^{\infty} J_s(\varphi_1)\cos(\omega_B+s\omega_u)t. \tag{8}$$

For small values of φ_1 and A_1/A_0, keeping only the carrier and the first lateral bands of the frequency spectrum,

$$V_{\text{det}}=A_0\{\cos\omega_B t+(\varphi_1/2)[\cos(\omega_B+\omega_u)t - \cos(\omega_B-\omega_u)t]\}+(A_1/2)\{\cos[(\omega_B+\omega_u)t+\phi] + \cos[(\omega_B-\omega_u)t-\phi]\}. \tag{9}$$

The term proportional to A_0 represents the carrier and the first sidebands in the absence of amplitude modulation. The second term affects the amplitude and the phase of the first sidebands. Depending on the value of ϕ, the amplitude difference of the two lateral bands relative to the carrier amplitude can be as large as A_1/A_0.

When Eq. (7) is substituted into Eq. (3), we obtain

$$V_u=-(\varphi_1/2)[A_0+A_1\cos(\omega_u t+\phi)]\sin\omega_u t$$
$$=-\frac{\varphi_1}{2}\left[A_0\sin\omega_u t-\frac{A_1}{2}\sin\phi+\frac{A_1}{2}\sin(2\omega_u t+\phi)\right]. \tag{10}$$

The demodulated signal contains an additional dc level and a second harmonic equal to $A_1/2A_0$ times the fundamental amplitude. This ratio is typically a few percent for acoustic amplitudes of about 100 Å and is comparable to the second harmonic amplitude generated in most solids.

To remove the effects associated with amplitude modulation, V_{det} is converted into a phase-modulated square wave, V_{sq}, using a comparatorlike circuit. This circuit maintains V_{sq} at a constant amplitude if V_{det} is larger than some minimum value. The system is therefore largely insensitive to variations in the amount of collected light or to amplitude modulations of V_{det}.

The phase-modulated V_{sq} can be written as a phase-modulated Fourier expansion of a square wave:

$$V_{\text{sq}}=\frac{4}{\pi}\sum_{n=1,n\ \text{odd}}^{\infty}\frac{1}{n}\cos n(\omega_B t+\varphi(t)). \tag{11}$$

Replacing $\varphi(t)$ by $\varphi_1\sin\omega_u t$ and using Eq. (5), V_{sq}, reduces to

$$V_{\text{sq}}=\frac{4}{\pi}\sum_{n=1,n\ \text{odd}}^{\infty}\sum_{s=-\infty}^{\infty}\frac{J_s(n\varphi_1)}{n}\cos(n\omega_B+s\omega_u)t. \tag{12}$$

Such a frequency spectrum is shown in Fig. 3. Only odd harmonics of the carrier are present and they decrease in amplitude as $1/n$. Each of these harmonics is phase modu-

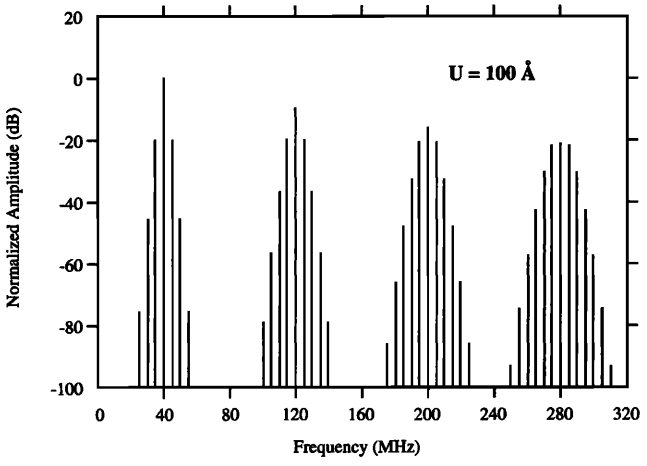

FIG. 3. Frequency spectrum of V_{sq} for $\omega_B=40$ MHz, $\omega_u=5$ MHz, and $U_1=100$ Å ($\varphi_1=0.2$).

lated with lateral bands of relative amplitude equal to $J_s(n\varphi_1)$. Note that the relative intensities of the (fundamental) carrier and of its sidebands, the $n=1$ term in the expansion, are unchanged from Eq. (4). When V_{sq} is used as the input of the demodulation circuit of Fig. 2, the higher-order harmonics of the carrier and their sidebands are mixed with the 40-MHz frequency of the VCXO. The non-negligible (i.e., those with small enough values of s) additional components of the mixer output produced are all above the carrier frequency, ω_B, and are removed by the output low-pass filter. Therefore, the output signal, V_u, reduces to that of Eq. (6), and all problems associated with unsteady calibrations and amplitude modulation of the carrier frequency are eliminated.

B. Distortions of the comparator circuit

There are three principal sources of distortion introduced by the comparator (and detector) circuit: second harmonic generation and frequency dependence of the gain and propagation delay. The comparator circuit may generate second (and higher) harmonics of its input signal and, in particular, of the carrier frequency and its sidebands. When mixed with the in-quadrature signal, these harmonics produce a signal below ω_B that appears like peaks in the noise spectrum. If the acoustic signal has a narrow bandwidth, this extra noise can often be filtered out. In general, the second harmonic generation can be controlled by maintaining the comparator's input signals at relatively low levels.

Frequency variations of the gain and of the propagation delay are more serious difficulties. The mixer is an element producing output frequencies at the sum and difference of its two input frequencies. Therefore, when V_{det} is mixed with the VCO quadrature signal, the positive and negative sth sidebands yield signals of frequencies $\pm s\omega_u$. Because of their phases, the positive and negative sidebands add for odd values of s and cancel for even values of s. The precise cancellation of the even harmonics, however, is possible only if the comparator circuit and any other component between the photodetector and the mixer do not alter the relative phase and amplitude of these sidebands.

If the gain of the amplifier at the frequency of the sideband s is $A_{\pm s}$ and if $A_{\pm s}=A_0+\Delta A_{\pm s}$, Eq. (6) becomes

$$V_u=-\sum_{s=1,s\ \text{odd}}^{\omega_B/\omega_u} A_0 J_s(\varphi_1)\sin s\omega_u t - \frac{1}{2}\sum_{s=-\omega_B/\omega_u}^{\omega_B/\omega_u} \Delta A_s J_s(\varphi_1)\sin s\omega_u t. \tag{13}$$

The correction terms are in phase with the acoustic signal and affect the dc offset and all harmonics of the demodulated signal. For small values of φ_1, the ratio of the spurious second harmonic to the fundamental is equal to

$$\frac{V_{u2}}{V_{u1}}=\frac{\Delta A_2 J_2(\varphi_1)-\Delta A_{-2}J_{-2}(\varphi_1)}{2A_0 J_1(\varphi_1)}\approx\frac{\Delta A_2-\Delta A_{-2}}{8A_0}\varphi_1. \tag{14}$$

For $(\Delta A_2-\Delta A_{-2})/A_0=0.1$ dB (a value attainable with high quality amplifiers) and $U=100$ Å, $V_{u2}=0.029$ Å. Consequently, the frequency dependence of the gain can be controlled sufficiently well to contribute a negligeable amount to the total second harmonic signal.

If the propagation delay of the amplifier, Δt_s, is not constant as a function of frequency, phase shifts $\phi_s=(\omega_B+s\omega_u)\Delta t_s$ must be introduced in Eq. (6) and we find that

$$V_{sq}\sin\omega_B t=\sin\omega_B t\sum_{s=-\infty}^{\infty} J_s(\varphi_1)\cos((\omega_B+s\omega_u)t+\phi_s), \tag{15}$$

$$V_u=-\frac{1}{2}J_0(\varphi_1)\sin\phi_0-\frac{1}{2}\sum_{s=1}^{\omega_B/\omega_u} J_s(\varphi_1)\sin(s\omega_u t+\phi_s) - J_{-s}(\varphi_1)\sin(s\omega_u t-\phi_{-s}).$$

Assuming that $\phi_s\ll 1$ and choosing $\phi_0=0$, V_u reduces to

$$V_u=-\sum_{s=1,s\ \text{odd}}^{\omega_B/\omega_u} J_s(\varphi_1)\sin s\omega_u t+\frac{1}{2}\sum_{s=1}^{\omega_B/\omega_u}(\phi_s J_s(\varphi_1) + \phi_{-s}J_{-s}(\varphi_1))\cos s\omega_u t. \tag{16}$$

The correction terms affect all harmonics of the demodulated signal but they are 90° out of phase with the acoustic signal. For small values of φ_1, the ratio of the spurious second harmonic to the fundamental is equal to

$$\frac{V_{u2}}{V_{u1}}=\frac{\phi_2 J_2(\varphi_1)+\phi_{-2}J_{-2}(\varphi_1)}{2J_1(\varphi_1)}\approx(\phi_2+\phi_{-2})\frac{\varphi_1}{8}. \tag{17}$$

In Eqs. (15)–(17), ϕ_s are the phase shifts due to the variation between the propagation delays at the frequency of the sideband considered and at the carrier frequency ω_B. Therefore, the consistency of the propagation delay is more important at high frequencies because a small variation in time delay leads to a larger phase shift. For $\phi_2=\phi_{-2}=25$ mrad (100 ps at 40 MHz) and $U=100$ Å, $V_{u2}=0.12$ Å. Since few amplifiers are capable of keeping the propagation delay constant to this precision, this source of second harmonic generation is perhaps the most serious of those investigated here. Addi-

tionally, the photodetector capacitance creates an unavoidable low-pass filter that affects the uniformity of the propagation delay. To reduce this problem, a 350-MHz silicon photodiode is used as a photodetector.

C. Phase error of the quadrature signal

If the angle between the quadrature signal and V_{det} or V_{sq} differs from 90° by an amount ϕ in Eq. (6), then V_u becomes

$$V_u=\frac{1}{2}\sin\phi\, J_0(\varphi_1)-\cos\phi\sum_{s=1,s\ \text{odd}}^{\omega_B/\omega_u} J_s(\varphi_1)\sin s\omega_u t$$

$$+\sin\phi\sum_{s=2,s\ \text{even}}^{\omega_B/\omega_u} J_s(\varphi_1)\cos s\omega_u t. \tag{18}$$

This phase error introduces a dc offset of amplitude $\frac{1}{2}\sin\phi\, J_0(\varphi_1)$ and even harmonics of amplitude $\sin\phi\, J_s(\varphi_1)$ which are phase shifted by 90°. For small φ_1 and ϕ,

$$\frac{V_{u2}}{V_{u1}}=\frac{J_2(\varphi_1)\sin\phi}{J_1(\varphi_1)\cos\phi}\approx\phi\frac{\varphi_1}{4}. \tag{19}$$

Note that Eq. (18) is a special case of Eq. (15) for $\phi_{\pm s}=\phi_0=\phi$. For a fundamental amplitude of 100 Å and $\phi=1°=17$ mrad, the electronics generates a second harmonic with amplitude of 0.09 Å. Since this signal is a substantial fraction of the second harmonic that may be generated by the material, the quadrature angle must be adjusted to better that one degree.

Here, V_{sq} is mixed with the in-quadrature signal and the output, V_u, is filtered to retain only the dc component. The difference between the dc voltage and a reference voltage is used in a feedback loop to adjust the phase (frequency) of the VCO until the dc output of the mixer equals the reference voltage (see Fig. 2). For an ideal mixer, quadrature detection occurs for a zero reference voltage. In practice, the mixer and the difference amplifier have dc offsets so that the reference voltage must be adjusted to a nonzero value. To find the proper reference voltage, the feedback loop is unlocked and the dc level of V_u is measured. Then the feedback loop is locked again and the reference voltage is adjusted until the dc level of V_u equals the previously measured value.

D. Mechanical vibrations and laser fluctuations

The feedback loop compensates for low-frequency mechanical vibrations and maintains the phase of the quadrature signal. Because some residual dc offset must be present to drive the loop, the fluctuations in the dc offset caused by mechanical vibrations are reduced by a factor equal to the gain of the loop at the frequencies considered. The remaining error signal corresponds to a time-varying phase $\phi(t)$ that produces a varying amount of second harmonics. The situation, however, is improved by increasing the gain of the loop and mechanically isolating the interferometer. As mentioned in Sec. I, one advantage of the heterodyne interferometer is that the quadrature is maintained electronically. Consequently, larger gains and better tracking can be obtained than with homodyne interferometers which must use a movable mechanical component. Moreover, because the sign and amplitude of vibration-induced second harmonics are uncorrelated in time, time averaging techniques can reduce these harmonics greatly.

Our interferometer uses a multimode, 10 mW He–Ne laser. The modes are unstable and shift in frequency to create a ≈50-kHz phase noise similar but of higher frequencies than the noise produced by mechanical vibrations. The feedback loop cannot compensate for this high-frequency noise. This problem can be reduced if the probe and reference beam path lengths are equal or if a single mode laser is used. This laser noise contributes to second harmonic generation but, as for mechanical vibrations, the sign and amplitude of these harmonics are uncorrelated in time and time averaging techniques can reduce these harmonics greatly.

E. On the use of mixers

Mixers are highly nonlinear elements. They distort the expected output because of their dc offset, harmonic generation, two-tone intermodulation, and imperfect isolation of the input ports. These problems, however, can be reduced by saturating the Lo input port and sufficiently reducing the amplitude at the rf input port.

F. Signal-to-noise ratio

Because the second harmonic amplitude is much smaller than the fundamental amplitude, and because the sensitivity of optical detection techniques is less than that of other techniques, the second harmonic is usually hidden in the wideband noise. As with all other optical techniques, the signal-to-noise ratio can be improved by increasing the amount of detected light and reducing the detection bandwidth.[15] Signal averaging also works well. With the current system, second harmonic amplitudes smaller than 0.05 Å superposed onto a fundamental amplitude of 80 Å or more can be detected.

G. On the use of amplifiers and digitizers

All amplifiers generate an amount of second harmonics proportional to the square of the amplitude of the fundamental frequency. Therefore, if the output amplifier is operated with electric signals that are small enough, its second harmonic contribution will be negligible.

Digitizers have limited dynamic ranges (e.g., a 12-bit ADC has a dynamic range of 72 dB at best) and nonlinear responses at the level of precision required here. It is therefore imperative to separate the fundamental from the second harmonic components of V_u with analog filters, and to digitize both signals separately so that any harmonics produced by the digitization of the large-amplitude fundamental will not be superposed to the acoustic small-amplitude second harmonic. Consequently, numerical filtering of the wideband signal must be avoided.

H. Calibration of the interferometer

There are three possible methods to calibrate the interferometer. In the first method, a sample is excited with a continuous acoustic wave of amplitude U_0. The frequency

content of V_{det} is analyzed using a calibrated spectrum analyzer. The amplitude ratio of the first sidebands [$s=\pm 1$ in Eq. (4)] to the carrier is equal to $J_1(\varphi)/J_0(\varphi)\approx\varphi/2 \approx 2\pi U_0/\lambda$ for $\varphi\ll 1$. This measurement of the acoustic displacement is compared to V_u and provides a calibration of the interferometer.[16] Because the displacement can be obtained directly from the photodiode's current signal without any further electronic processing, this method should be the most reliable. It, however, requires a spectrum analyzer able to measure amplitudes to 0.1 dB accuracy for 1% accuracy in the calibration. Additionally, the previously discussed amplitude modulation of V_{det} introduces a source of error in the measurement of the first sidebands [see Eq. (9)]. For best results, this calibration should be made using V_{sq} instead of V_{det}.

If the feedback loop of Fig. 2 is opened, the VCO frequency does not exactly match the Bragg frequency. The phase error ϕ fluctuates through 2π and V_u oscillates between $\pm V_{max}$ which is equal to $-A/2$ in Eq. (3). Therefore, the interferometer calibration at $\phi=0$ is given by

$$\frac{V_u(t)}{V_{max}}=\sin\varphi(t)\approx\frac{4\pi U(t)}{\lambda}. \tag{20}$$

A third method relies on the relationship between the phase and the mixer's dc output. From Eq. (18), it can be seen that measuring $dV_u/d\phi$ at $\phi=0$ and $\varphi=0$ gives V_{max}:

$$\left.\frac{dV_u}{d\phi}\right|_{\phi=0}=V_{max} \tag{21}$$

and

$$\frac{V_u(t)}{[dV_u/d\phi]_{\phi=0}}\approx\varphi(t)=\frac{4\pi U(t)}{\lambda}. \tag{22}$$

For $\phi_0=0$, this calibration method gives the same results as Eq. (20) because $dV_u/d\phi|_{\phi=0}$ is equal to V_{max} for a sine waveform. In the general case, the mixer's output is related to the phase of its two inputs through the function $V_u(\phi+\varphi)$. This function can be measured by unlocking the feedback loop: If no acoustic displacement is present ($\varphi=0$), ϕ varies from 0 to 2π linearly (as long as the VCO's frequency stabilizes to a fixed frequency) and $V_u(\phi+\varphi)$ is easily measured. Any linear portion of $V_u(\phi)$ can be chosen to demodulate V_{det}. In this case (and for small acoustic displacements), the calibration is

$$\frac{V_u(t)}{[dV_u/d\phi]_{\phi=\phi_0}}=\frac{4\pi U(t)}{\lambda}. \tag{23}$$

Given their range of applicability, the three calibration methods are experimentally self-consistent. The third method is perhaps preferable because it does not require a spectrum analyzer and works even if the mixer's output is slightly distorted. Note that when the two input signals are square waves, the mixer's output is linearly related to its inputs' phase difference. Although this would seem advantageous because no precise adjustment of the quadrature phase would be required, the square waves are often distorted and the mixer's output is only approximately linear.

III. DISCUSSION AND EXPERIMENTAL RESULTS

To verify that the interferometer and associated electronics operate according to the model described by Eq. (18), we measured the following five quantities of V_u as a function of ϕ in a suprasil W1 (fused quartz) sample: dc offset, fundamental amplitude and phase, and second harmonic amplitude and phase. Suprasil W1 was chosen because of its relatively large nonlinearity and sample to sample reproducibility as measured by other authors. The sample was a cylinder of one inch diameter and $\frac{1}{2}$ in. in length. A 4.9-MHz, 1-in.-diam, $LiNbO_3$ transducer was bonded with oil to one of the two flat faces. The other face was coated with Al to increase the amount of probe light reflected. The measurement was performed in the near acoustic field whereby the Fresnel parameter (equal to $\lambda z/a^2$, where λ is the acoustic wavelength, z is the distance traveled by the acoustic wave, and a is the radius of the transducer's active region)[17] for this geometry was equal to 0.08. It was also experimentally verified that the fundamental amplitude of the first echo was uniform over a large area near the center of the detection surface.

Given the additional contribution of the sample nonlinearities to the second harmonic, Eq. (18) must be rewritten as

$$V_u=2V_{max}((\sin\phi/2)J_0(\varphi_1)+\cos\phi J_1(\varphi_1)\sin\omega_u t + \sin\phi J_2(\varphi_1)\cos 2\omega_u t+\cos\phi J_1(\varphi_2)\sin 2\omega_u t), \tag{24}$$

where φ_1 and φ_2 correspond to the phase shifts due to the acoustic fundamental and second harmonic, respectively. The dc offset, the fundamental amplitude and phase, and the second harmonic amplitude and phase as a function of ϕ, are given the respective symbols V_{u0}, V_{u1}, θ_1, V_{u2}, and θ_2, and are fitted to the following equations:

$$V_{u0}=V_{max}\sin(\phi-\phi_0)J_0(\varphi_1)+V_0,$$

$$V_{u1}=2V_{max}\cos(\phi-\phi_0)J_1(\varphi_1),$$

$$\theta_1=\text{a constant},$$

$$V_{u2}=2V_{max}\sqrt{(\sin(\phi-\phi_0)J_2(\varphi_1))^2+(\cos(\phi-\phi_0)J_1(\varphi_2))^2},$$

$$\theta_2=\arctan\left(\frac{\sin(\phi-\phi_0)J_2(\varphi_1)}{\cos(\phi-\phi_0)J_1(\varphi_2)}\right)+\theta_0, \tag{25}$$

where V_0 is some offset voltage, and ϕ_0 and θ_0 are arbitrary phases. To perform these measurements, the quadrature phase error, ϕ, is selected by varying the reference voltage of the feedback loop. The least-squares fits and the measured values are shown in Fig. 4 (to the accuracy of the measurement, θ_1 is constant and is not shown). The voltage amplitudes are as measured and the scales do not match because of the various electronic gains. Each of the four graphs is fitted independently of the other three. The fitted parameters are compared in Table I where they have been corrected for the various electronic calibrations and gains.

Table I also shows the values of the parameters obtained during calibration. Section II discusses how the calibration of the interferometer yields a value of V_{max}. Of the three calibration methods discussed, the last two were applied: Measuring the amplitude (method II) and the slope at zero output voltage (method III) of the interferometer's low-frequency

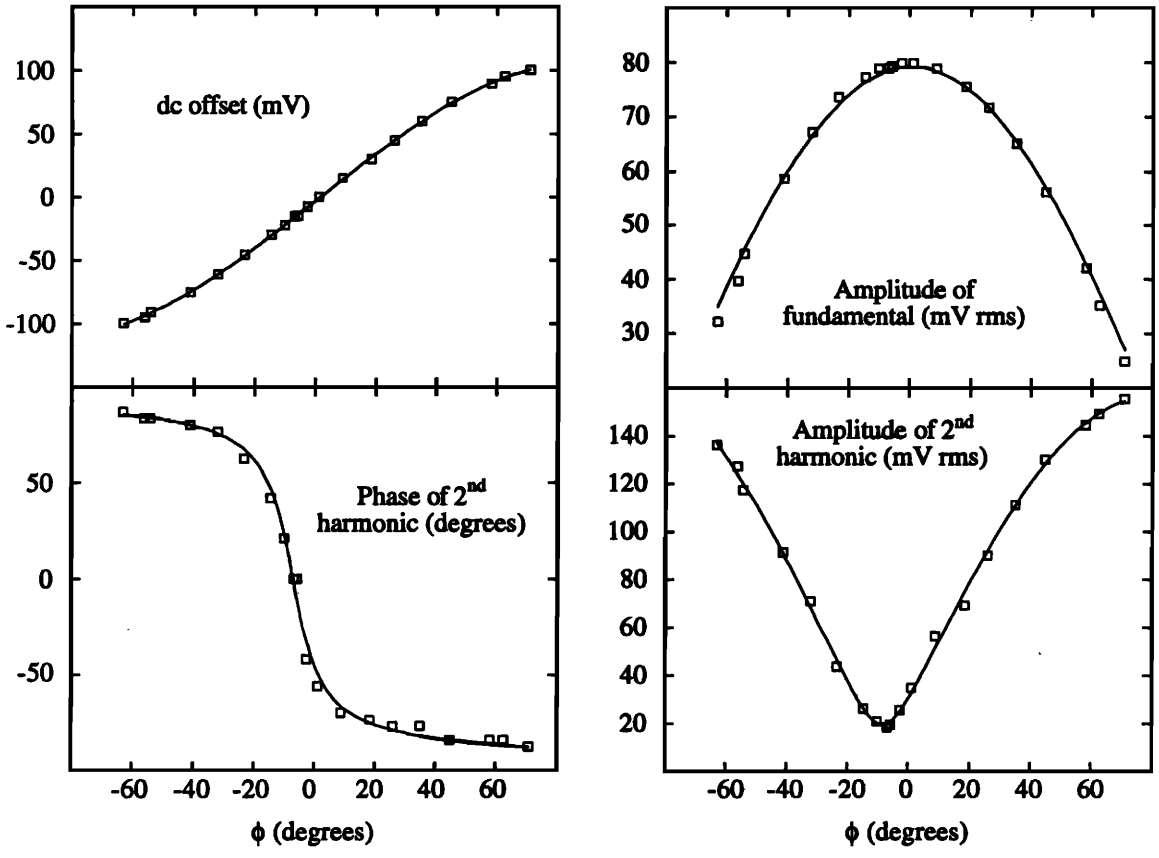

FIG. 4. dc offset, fundamental amplitude, and second harmonic amplitude and phase of V_u as a function of ϕ in a suprasil W1 sample. The squares are the measured values and the solid lines are least-squares fits to subexpressions of Eq. (25). The phase difference, ϕ, is determined from the least-squares fit to the dc offset measurements. The abscissa do not match and the fitted parameters are shown in Table II.

oscillations when the feedback loop is unlocked. These two calibrations are in excellent agreement with the value of $V_{\max}$ obtained from V_{u0} (see Table II). The dc component of V_u when the loop is unlocked is converted to ϕ_0 and compared to values of ϕ_0 found from the graphs of V_{u1} and θ_1: these values agree to within one degree. The two values of ϕ_0 extracted from V_{u2} and θ_2, however, agree well between themselves but differ significantly from the previous three. The two fitted values of φ_1 also agree between themselves.

The model describing the interferometer is essentially valid but the presence of two different values of ϕ_0 is troublesome. In the previous section, it was seen that nonuniform gains in processing $V_{\det}$ could lead to a spurious second harmonic that was in phase with the acoustic second harmonic. It was also seen that two other sources of spurious second harmonics, the nonuniform propagation delays of $V_{\det}$ and the phase error of the quadrature signal, generate second harmonics that are 90° out of phase with the acoustic second harmonic (see Table II). Of these three sources, the nonuniform propagation delays of $V_{\det}$ was estimated to have the largest contribution. If all spurious sources of second harmonics are small, then the quadrature phase error can be adjusted so that the sources that are 90° out of phase with the acoustic signal cancel each other. In this case, a plot of V_{u2} as a function of ϕ may show a minimum for a value of ϕ_0 different from the one for which the maximum of V_{u1} oc-

TABLE I. Various parameters extracted from the fitted curves shown in Fig. 4, from two calibration procedures, and from unlocking the phase-locked loop.

Measurement	$V_{\max}$ (mV)	φ_1 (radian)	φ_2 (radian)	ϕ_0 (deg)
Calibration II	109.8	···	···	···
Calibration III	108.8	···	···	···
Loop unlocked	···	···	···	0.7
dc offset (V_{u0})	109.5	···	···	0.0±0.5
Fundamental amplitude (V_{u1})	···	0.165	···	0.6±0.4
Harmonic amplitude (V_{u2})	···	0.173	9.3×10^{-4}	−7.7±0.4
Harmonic phase (θ_2)	···	···	···	−7.2±0.4

TABLE II. Summary of second harmonic contributions for a sinusoidal acoustic excitation of frequency ω_u.

Source	Magnitude	Phase
Acoustic	$J_1(\varphi_2)\cos\phi$	0°
Uniformity of gain of $V_{\det}$	$(\Delta A_2-\Delta A_{-2})J_2(\varphi)$	0°
Uniformity of phase of $V_{\det}$	$(\sin\phi_2+\sin\phi_{-2})J_2(\varphi)$	±90°
Quadrature phase error	$J_2(\varphi_1)\sin\phi$	±90°
Output amplifier distortion	$C\varphi_1^2$	0°

curs. This would explain the two different values of ϕ_0 observed in Table I. If this is true, then the interferometer should be operated at the value of ϕ_0 obtained using V_{u2} and θ_2 when measuring second harmonic generation. Moreover, because the acoustic fundamental and second harmonic varies as the cosine of ϕ, the small adjustment in ϕ_0 used to cancel spurious second harmonics does not affect the acoustic measurements significantly. In the case presented in Fig. 4 and Table I, the discrepancy of about 8° corresponds to an error of only 1% in the measured acoustic fundamental and second harmonic amplitudes. Alternatively, additional terms were added to Eq. (24) to attempt to model some of these nonlinearities. The results were inconclusive because these terms are not sufficiently independent from those already mentioned or from each other.

The spurious second harmonics that would be in phase with the acoustic second harmonic (the most important one being the nonuniform gains in processing V_{det}) cannot be canceled out in a manner similar to the spurious harmonics that are in quadrature. Therefore, these contributions will be considered negligible if the measured nonlinearity parameter of the Suprasil sample agrees with values found in the literature. The values of φ_1 and φ_2 extracted from Fig. 4 yield a fundamental surface amplitude of 83 Å and a second harmonic amplitude of 0.46 Å (the bulk amplitudes are half these values). The corresponding absolute value of the nonlinearity parameter β is 13.7.

In another series of experiments, the interferometer was set to operate at the value of ϕ_0 that minimized the second harmonic amplitude. Measurements were made at 4.9, 7.4, and 10.0 MHz, in samples 0.25 and 0.5 in. thick, with acoustic amplitudes ranging from 3 to 6 nm, and by three different experimenters. The average and standard deviation of these measurements yielded $|\beta|=13.4\pm1.2$. The result is in reasonable agreement with the values $\beta=-11.6$ (Ref. 18) and -12.7 (Ref. 4) quoted in the literature. Therefore, the contribution of the spurious second harmonics that are in phase with the acoustic second harmonic are small and we believe that the interferometer gives a reliable measurement of the second harmonic amplitude.

IV. CONCLUSION

We measured the nonlinearity parameter β of suprasil W1 using a heterodyne interferometer to detect the absolute displacement of the sample's surface. The interferometer can detect second harmonic amplitudes smaller than 0.05 Å superposed onto fundamental amplitudes greater than 80 Å (dynamic range >64 dB). The main advantages of this method are the speed at which the measurements are made and the small amount of sample preparation required. In principle, one could measure samples with rough surfaces and *no* sample preparation if a sufficiently powerful detection laser were used. Moreover, the method allows for point detection of surface motion, in contrast to capacitive or piezoelectric detection methods that average the acoustic signal over a large area. This characteristic has permitted the detailed measurement of the second harmonic displacement field.[19] Although this interferometer is still a laboratory instrument, it could be an important technological advance toward industrial applications of nonlinear acoustics.

ACKNOWLEDGMENTS

The author thanks Jean-Pierre Monchalin and J. Bussière for helpful discussions and Martin Lord for invaluable technical assistance. This work was supported in part by the CANDU Owner's Group.

[1] For a recent review, see J. H. Cantrell and K. Salama, "Acoustoelastic characterization of materials," Int. Mater. Rev. **36**, 125–145 (1991).
[2] M. A. Breazeale and J. Philip, "Determination of third-order elastic constants from ultrasonic harmonic generation measurements," in *Physical Acoustics*, Vol. 17, edited by W. P. Mason and R. N. Thurston (Academic, New York, 1984), p. 1–60.
[3] P. Li, W. P. Winfree, W. T. Yost, and J. H. Cantrell, Jr., "Observation of collinear beam-mixing by an amplitude modulated ultrasonic wave in a solid," *Proceedings of the IEEE Ultrasonics Symposium*, Cat No. 82CH1947-1, edited by B. R. McAvoy (Institute of Electrical and Electronics Engineers, New York, 1983), pp. 1152–1156.
[4] W. T. Yost and J. H. Cantrell, Jr., "Acoustic-radiation stress in solids. II. Experiment," Phys. Rev. B **30**, 3221–3227 (1984).
[5] W. B. Gauster and M. A. Breazeale, "Detector for measurement of ultrasonic strain amplitudes in solids," Rev. Sci. Instrum. **37**, 1544–1548 (1966).
[6] E. G. Lean, C. C. Tseng, and C. G. Powell, "Optical Probing of Acoustic Surface-Wave Harmonic Generation," Appl. Phys. Lett. **16**, 32–35 (1970).
[7] For a review, see G. I. Stegeman, "Optical Probing of Surface Waves and Surface Wave Devices," IEEE Trans. Sonics Ultrason. **23**, 33–63 (1976).
[8] D. Doughty, "A laser interferometer technique for measuring sound harmonic distortion in the acoustic output of a transducer," Report No.: TM-681-02, Pennsylvania State Univ., Institute for Science and Engineering, Ordinance Research Lab., University Park, PA. (27 March, 1970).
[9] B. A. Auld, S. Ayter, and M. Tan, "Filter Detection of Phase-Modulated Laser Probe Signals," Electron. Lett. **17**, 661–662 (1981).
[10] Yutaka Abe and Kazuaki Imai, "Interferometric measurement of the third-order elastic constants in germanium and gallium arsenide," *Proceedings of the IEEE Ultrasonics Symposium*, Cat No. 85CH2209-5, edited by B. R. McAvoy (Institute of Electrical and Electronics Engineers, New York, 1985), pp. 1109–1112.
[11] Xie Wenxiang, "Sonde hétérodyne laser à résolution optimisée pour les mesures d'ondes de surface en propagation non linéaire et en milieu multicouche," Doctoral thesis, Université de FRANCHE-COMTE, 1988.
[12] A. Moreau and J. Bussière, "Detection of acoustic second harmonics using a laser interferometer," *Rev. Prog. in Quant. Nondest. Eval.*, edited by D. O. Thompson and D. E. Chimenti (Plenum, New York, 1993), Vol. 12, pp. 2051–2058.
[13] J. P. Monchalin, R. Héon, and N. Muzak, "Evaluation of Ultrasonic Inspection Procedures by Field Mapping with an Optical Probe," Can. Metall. Q. **25**, 247–252 (1986).
[14] J.-P. Monchalin, J.-D. Aussel, R. Héon, C. K. Jen, A. Boudreault, and R. Bernier, "Measurement of in-plane and out-of-plane ultrasonic displacements by optical heterodyne interferometry," J. Nondest. Eval. **8**, 121–133 (1989).
[15] J.-P. Monchalin, "Optical detection of ultrasound," IEEE Trans. Ultrason. Ferromagn. Freq. Control **33**, 485–499 (1986).
[16] G. Bouchard and D. B. Bogy, "Experimental measurement of scattered surface waves using a laser-Doppler technique," J. Acoust. Soc. Am. **77**, 1003–1009 (1985)
[17] J.-D. Aussel and J.-P. Monchalin, "Measurement of ultrasound attenuation by laser ultrasonics," J. Appl. Phys. **65**, 2918–2922 (1989).
[18] J. H. Cantrell, Jr., and M. A. Breazeale, "Ultrasonic investigation of the nonlinearity of fused silica for different hydroxyl-ion contents and homogeneities between 300 and 3 °K," Phys. Rev. B **17**, 4864–4870 (1978).
[19] A. Moreau and J.-D. Dai (unpublished).